Aggregation of magnetic microparticles in the context of targeted therapies actuated by a magnetic resonance imaging system

Jean-Baptiste Mathieu[a] and Sylvain Martel[b]
Department of Computer and Software Engineering, NanoRobotics Laboratory, Ecole Polytechnique de Montreal (EPM), P.O. Box 6079, Station Centre-ville Montreal, Quebec H3C 3A7, Canada

(Received 4 February 2009; accepted 4 June 2009; published online 18 August 2009)

A study of magnetic aggregation in the context of magnetic resonance imaging (MRI) based actuated targeting is proposed. MRI systems can induce displacement forces on magnetized particles as they flow through the blood vessels. Magnetic aggregation of the particles happens when they are placed within the magnetic field of the MRI system and can greatly influence the MRI steering dynamics of magnetic particles. In this paper, a review of the different parameters that can be used to tailor the size, geometry, stiffness, and density of magnetic aggregates is proposed. Then, magnetic aggregation experiments on a suspension of Fe_3O_4 microparticles ranging from 0.1 to 100 μm in diameter are described. The effects of particle concentration, flow rate, and magnetic field amplitude were evaluated. Field amplitudes of 1.5 mT, 0.4 T, and 1.5 T fields were applied without any magnetic steering gradients and caused aggregates that could sometimes exceed 1 mm in length. Since magnetic aggregates can reach higher magnetophoretic velocities than individual particles, large aggregates could be exploited in larger arteries with important blood flows. A few strategies are discussed to assist in the design of MRI steering experiments by enhancing the positive effects of magnetic aggregation over its negative effects. © *2009 American Institute of Physics*. [DOI: 10.1063/1.3159645]

I. INTRODUCTION

Magnetic fields can be used to tailor the properties of a magnetic suspension over a wide range of amplitudes and directions. The formation of anisotropic magnetic aggregates leads to modification of the rheological,[1,2] optical,[3] and magnetic properties[4,5] of the suspension. An interesting investigation was published recently,[6] which describes rheological measurements on magnetic field induced chain formation of magnetic nanoparticles and discusses the effects of particles sizes and magnetic properties, magnetic field amplitude, and interactions with the walls of a viscometer.

Applications of the body force acting on a ferrofluid are liquid sealants, heat dissipation, magnetic separation, high speed printing, and drug targeting.[7] Magnetic targeting aims at using magnetic particles as drug carriers and directing them with magnetic fields with the intention of increasing the drug dosage in the targeted region and lowering it in the healthy tissues. Conventionally, external magnets are used to attract magnetic particles in a selected region.[8–13] Magnetic resonance imaging (MRI) systems can be used to improve the targeting of magnetic microparticles. Actually, the magnetic gradient coils used for slice selection and image encoding in MRI can also be used to apply three-dimensional (3D) steering forces on magnetized particles. These gradient coils offer constant force over regions as wide as 50 cm in the center of the MRI bore. Moreover, the MRI excellent sensitivity to magnetic susceptibility differences allows the use of standard imaging techniques to detect and track magnetic carriers as they are being injected and targeted.[14] The combination of the actuation force and tracking feedback information with real-time interventional software architecture of a modern MRI system makes it possible to put into action closed loop control over the position of a particle cloud or bolus. MRI targeting is an elegant approach that relies on a single platform, a single frame of reference, and a single software architecture to control the trajectory of a bolus of magnetic carriers through the cardiovascular system.[15–19]

The present work aims at evaluating the effects of magnetic aggregation and at identifying the parameters that can be used to influence the geometry, volume and density of magnetic aggregates, and hence affecting their magnetophoretic velocity and the dynamics of MRI steering.

II. BACKGROUND

A. Dynamics of MRI steering

The propulsion force induced by an MRI system on a magnetic particle or aggregate (MRI steering force) is given by

$$\vec{F}_{\text{mag}} = (\vec{m} \cdot \nabla)\vec{B} = V_{\text{ferro}} \cdot (\vec{M} \cdot \nabla)\vec{B}, \tag{1}$$

where $\vec{F}_{\text{mag}}$ is the magnetic force (N), $\vec{m}$ is the magnetic moment of the ferromagnetic body (A m^2), $\vec{M}$ is the magnetization of the material (A/m), V_{ferro} is the volume of the ferromagnetic body (m^3), $\vec{B}$ is the magnetic field (T), and ∇B is the gradient or spatial variation of the magnetic field (T/m).

[a]Author to whom correspondence should be addressed. Tel.: 514-340-4711 No. 5029. FAX: 514-340-5280. Electronic mail: jean-baptiste.mathieu@polymtl.ca.
[b]Electronic mail: sylvain.martel@polymtl.ca.

The viscous drag force acting on a particle is

$$F_f = fU, \tag{2}$$

where U is the velocity difference (or relative velocity) between the particle and the fluid and f is the friction coefficient. From Stoke's law of friction, in the case of a spherical particle,

$$f = 6\pi\mu a. \tag{3}$$

In Eq. (3), a is the radius of the sphere and μ is the viscosity of the fluid. Friction factors for such shapes as cylinders and spheroids are available in the literature. Nevertheless, magnetically aggregated particles often depart from simple analytical shapes. In this case, the aggregated particle is assimilated to a spherical particle with hydrodynamic radius a_h. The hydrodynamic radius is the radius of a hypothetical sphere that experiences the same friction force as the actual nonspherical particle. The friction tensor $[f]$ of nonspherical magnetic aggregates describes the resistance to flow of nonspherical particles in three dimensions.

$$[f] = \begin{bmatrix} f11 & 0 & 0 \\ 0 & f22 & 0 \\ 0 & 0 & f33 \end{bmatrix} = 6\pi\mu \begin{bmatrix} a_{h11} & 0 & 0 \\ 0 & a_{h22} & 0 \\ 0 & 0 & a_{h33} \end{bmatrix}. \tag{4}$$

In Eq. (4) magnetic clusters are regarded as nonspherical particles with their long axis oriented along the direction of the main magnetic field. They can be considered as having a different hydrodynamic radiuses for each direction of space. In the context of drug targeting, magnetic forces are used to guide drug loaded magnetic particles. Application of an MRI steering force F_{mag} on a microparticle or a cluster will translate to magnetophoretic velocity U_{mag},

$$\vec{U}_{\mathrm{mag}} = \vec{F}_{\mathrm{mag}}[f]^{-1}. \tag{5}$$

Magnetic aggregation strongly affects the hydrodynamic interactions between the particles and the surrounding fluid since aggregates and individual particles volumes, densities, and shapes differ significantly. This conclusion is illustrated in a paper by Darton *et al.*,[20] where the authors manipulate and track agglomerates of superparamagnetic nanoparticles in real time using magnetic field gradients generated by MRI. They validate that the nanosized magnetic particles used form micron sized aggregates that can overcome the viscous drag force to move at high velocities. Considering the major influence magnetic aggregation has on the dynamics of MRI steering, a review of some of its important aspects is proposed in the following paragraphs.

B. Magnetic dipole-dipole interaction

Magnetic interaction originates from the magnetic fields and magnetic field gradients generated by magnetized particles in their surrounding space. The magnetic interaction force F_{magInt} is a dipolar force related to the magnetic potential V_{mag}, which is both a function of the distance between particles and the angle between the direction of the magnetic field and the centerline between the magnetic particles (a straight line through the centers of both particles) as given in

$$F_{\mathrm{magInt}} = -\frac{dV_{\mathrm{mag}}}{dr}, \tag{6}$$

$$V_{\mathrm{mag}} = -\frac{4\pi M_i a_i^3 M_j a_j^3}{9\mu_0\left(\frac{r}{a_i}\frac{a_i + a_j}{2}\right)^3}(1 - 3\cos^2\alpha), \tag{7}$$

where M_i and M_j are the magnetizations of particles i and j, respectively, with radiuses a_i and a_j and separated by distance r, α is the angle between the magnetic field direction and the particle centerline, and μ_0 is the magnetic permeability of vacuum.[21]

In the case of ferromagnetic particles, the magnetization M is a nonlinear function of the magnetic field amplitude. It can be obtained from a magnetization curve measured using a magnetic properties measuring system such as a vibrating sample magnetometer (VSM) for example. The strength of the magnetic interaction increases with the magnetization of the particles, hence with the magnetic field. Nevertheless, at high magnetic fields (of the order of 1 T), the magnetization reaches a plateau value called saturation magnetization (M_{sat}). Beyond this state, the magnetic attraction between particles cannot increase any further with the amplitude of the magnetic field.

The magnetic interaction force can be both attractive and repulsive depending on the orientation of the particles with regards to the direction of the magnetic field. Because of this sign dependence of the magnetic potential over particle orientation, when becoming magnetically aggregated, magnetic particles form chains that tend to orient themselves along the direction of the magnetic field.

The DLVO (Derjaguin, Landau, Verwey, Overbeek) theory predicts that the magnetic interaction potential becomes predominant over other colloidal interaction as the magnetic moment of the particles increases.[22] In general, the magnetic potential has a longer range in comparison to the van der Waals and electrostatic potentials.[23] Nevertheless, particle size is a parameter that modifies the balance between the magnetic potential and the other colloidal potentials. As a matter of fact, the magnetic force is proportional to particle volume, while the van der Waals and electrostatic forces are functions of the particles radius. Therefore, the magnetic potential decreases faster and becomes less influential as smaller particles are considered. In the context of this project where we rely on concentrated suspensions of relatively large and strongly magnetized particles in the intense field of an MRI system, the magnetic interaction overcomes the repulsive colloidal potentials and magnetic aggregation occurs.

Both experimental studies and computer simulation agree with the fact that strong dipole-dipole interaction results into short flexible chains, which amount and length grow with an increase in the concentration of the suspension and in the strength of the external magnetic field. Magnetic clusters grow using large particles as nuclei that capture the smaller particles.[24] Aggregates in real ferrofluids are made of a small number of large particles in the center and small particles at the edge.[25]

Polydispersity in size of the suspensions causes the aggregates formed to depart from a linear chain configuration.[24,25] It causes small particles to also be able to aggregate side by side rather than only in linear configuration. As a matter of fact the influence of the attractive interaction between large particles and small particles dominates over the influence of the repulsive interaction between small particles. Therefore, small particles that have been captured by larger ones can stand in a side by side configuration even though they tend to repel each other.[24]

A measurement of aggregate density is provided by the fractal dimension. In two dimensions it was found to vary between 1.0 and 1.6.[21] It decreases with increasing magnetic susceptibility or magnetic field but increases with particle concentration.

In the context of MRI steering of microparticles, perikinetic aggregation is expected to have little influence over aggregation because it is driven by Brownian motion, which only has a minor effect on micrometric particles. Instead, orthokinetic aggregation of the magnetized suspension takes place during MRI steering experiments while it is being injected in a channel. It is greatly influenced by the hydrodynamic flow and by external body forces such as the MRI steering force and gravity. Orthokinetic aggregation relies on unequal velocities of the particles (or aggregates) to facilitate particle captures and aggregate growth. A particle (or aggregate) and another particle (or another aggregate) moving with different velocities will have a chance to aggregate by penetrating within each other's magnetic capture volume.[26]

One possible cause for relative motion is the hydrodynamic flow of the suspending fluid during drug delivery inside arteries or within tubing or catheters. The viscosity of the fluid causes the flow velocity to vary along the transverse direction of the channel. This gradient of the velocity profile (or shear rate) causes suspended particles and aggregates to have different velocities depending on their position. In this case, the velocities of the particle are a function of the shear rate and a function of the distance separating them.

Gravity and the MRI steering force are both volumic forces that also induce relative motion and orthokinetic aggregation. In both cases, particles are in relative motion due to velocity differences caused by size polydispersity. For example, faster particles (or aggregates) sweep the fluid and capture particles (or aggregates) that come within range of the magnetic interaction force. The behavior of the particles under the influence of the MRI steering force can be compared to gravity induced sedimentation with the difference that its direction can be controlled. Comparing gravity and the MRI steering force implies that gradient amplitudes over approximately 160 mT/m (on Fe_3O_4 particles magnetized by a 1.5 T magnetic field) would be required to cause a magnetic force exceeding the gravitational attraction.

Determining the dominant cause of orthokinetic aggregation between the hydrodynamic flow or volumic force (gravity and magnetophoretic forces) is not straightforward because these effects depend on distinct parameters that can vary greatly and independently. Hence, the answer will depend on the experimental conditions and calibration is recommended to adjust aggregate size to the experimenter's requirements.

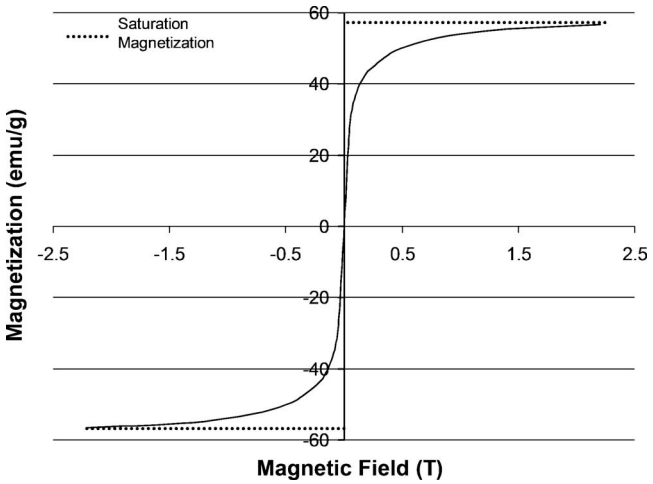

FIG. 1. Magnetization curve of Fe_3O_4 magnetic suspension.

Even though velocity differences can allow particles and aggregates to approach within the range of the magnetic attraction, the viscous forces (shear stress) exerted by the fluid on these aggregates tend to cause particle desorption. The balance between magnetically caused adsorption and shear induced desorption determines whether aggregate growth or breakdown occurs. This balance is quantified by the nondimensional Mason number Mn that represents the ratio of the shear forces to the magnetic forces,

$$Mn \propto \dot{\gamma}/(B/\mu_0)^2, \tag{8}$$

where $\dot{\gamma}$ is the rate of shear.[27,28]

For low values of the Mason number, shear will lead to an increase in aggregate size[26] while a reduction in aggregate size will occur at high values of the Mason number. In the context of MRI actuated targeted therapies, low Mason numbers and shear enhanced aggregation are encountered inside the bore of the MRI while high Mason numbers and shear induced aggregate breakdown occur when the patient or the setup exits the MRI bore.

III. MATERIALS AND METHODS

A. Magnetic suspension

A magnetic suspension (BioMag BM547, Bangs Laboratories, IN, USA, commercial concentration of 45 mg/ml) containing Fe_3O_4 magnetic particles in distilled water was used. The average particle diameter was 11 μm and the 25th and 75th percentile were 5 and 20 μm, respectively. The laser diffraction system used for size measurement (Malvern Mastersizer S, Worcestershire, U.K.) requires low concentrations of the order of 0.1–0.3 mg/ml. The volume size distribution that was measured is expected to be independent of the concentration. In this work, the suspending fluid is Deionized (DI) water. Figure 1 provides a magnetization curve of the Fe_3O_4 suspension used (Walker Scientific VSM, Worcester, MA, USA).

B. Electromagnet setup

A stereomicroscope (Stemi 11, Carl Zeiss GmbH, Germany) was adapted on an electromagnet (GMW 5403, Power and Buckley, New Zealand). The objective was positioned between both coils of the electromagnet and above the sample. The maximum magnetic field amplitude was 0.4 T (measured using a Lake Shore 450 Gaussmeter with a transverse hall probe (Lake Shore Cryotronics, Inc., OH, USA) and no magnetic steering gradient was applied. From Fig. 1, the magnetization of the suspension at $B=0.4$ T is $M_{0.4\ \mathrm{T}}=48.7$ emu/g. When the current was turned off, the ferromagnetic poles of the electromagnet kept a remanent field of the order of 1.5 mT. Several concentrations of the magnetic suspension were tested: 45, 4.5, 2.25, 1.13, and 0.56 mg/ml. The magnetic suspension was injected manually using a syringe in a 1 mm wide and 100 μm deep poly(methyl methacrylate) (PMMA) fluidic channel under the objective of the microscope. The magnetic field was then applied while low residual flow subsisted during the aggregation process. A video camera (DCR-HC1000, Sony, Japan) was fitted to the microscope and connected to a computer to record the aggregation behavior of the magnetic suspension. The pictures show the same particles before and after the electromagnet was turned on. Image analysis was performed over three images for each concentration using software SIGMASCAN (Systat Software Inc., San Jose, CA, USA). A few additional experiments were conducted in order to examine the effect of stronger flow on the aggregates. A flow was applied manually after aggregation had reached a stable state. The current in the electromagnet was either on or off during the injection.

C. MRI setup

The effect of higher magnetic field and constant shear was evaluated using an MRI setup. From Fig. 1, the magnetization of the suspension at $B=1.5$ T is $M_{1.5\ \mathrm{T}}=58$ emu/g. A Y-shaped fluidic channel made of PMMA with a rectangular cross section (length=20 mm, width=2.5 mm, depth =0.3 mm) was centered inside a 1.5 T Siemens Avanto scanner (Siemens, Erlangen, Germany) no magnetic steering gradient was applied. The main branch of the channel was oriented along the horizontal transverse axis of the MRI scanner (x axis) causing the flow to be orthogonal to the direction of the magnetic field there. Size measurements were carried out in the outlet branches where the angle between the flow and the magnetic field was +30° and −30° because lower flow velocity was present there, which improved measurement accuracy. The flow was generated by two syringe pumps (New Era Pump Systems, Inc., NY, USA) with an amplitude of 0.55 ml/min, which corresponds to an average velocity of 12.2 and 6.1 mm/s in the main branch and in the outlet branches of the channel respectively. The magnetic suspension with concentration 1.13 mg/ml was injected in the channel through a three way valve. An MRI compatible camera (MRC systems GmbH, Heidelberg, Germany) was fastened on top of the fluidic channel and recorded the behavior of the aggregated suspension as it was flowing through the channel. A light emitting diode was used for transmission lighting of the fluidic channel. Channel depth (0.3 mm) was chosen so that it was smaller than the depth of focus of the camera in order to monitor the entirety of the particulate flow. Manual aggregate size measurement over randomly selected frames from 5 experimental video files (10 frames per video file) was performed using the ZEISS AXIOVISION software (Carl Zeiss GmbH, Germany).

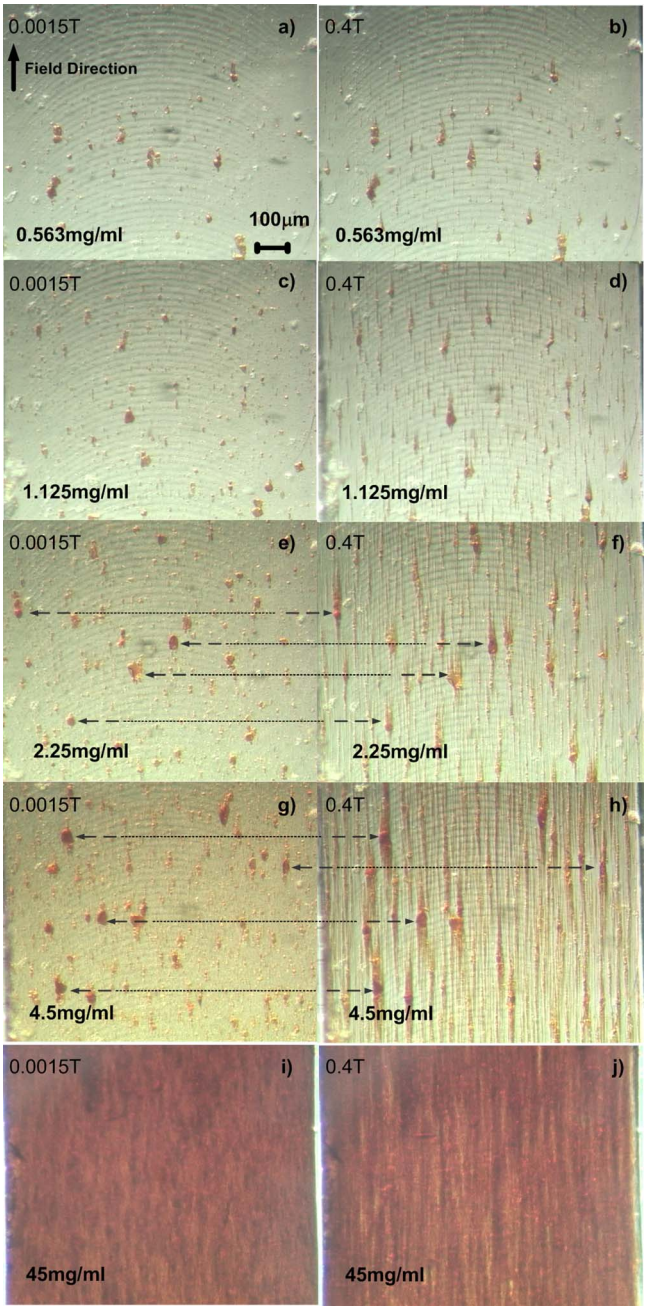

FIG. 2. (Color online) Effect of particle concentration and magnetic field amplitude on the magnetic aggregation of Fe_3O_4 microparticles.

IV. RESULTS

Figure 2 and video 1 show the images captured with the camera using the electromagnet setup. It provides data about the effects of particle concentration and magnetic field strength. No external magnetic gradient is applied during this experiment. Therefore, all particle movement is attributed to fluid motion, gravity, and magnetic interactions between the

particles. On the left hand side column of Fig. 2 (low field column), one can see the magnetic suspension with various concentrations in low magnetic interaction configuration (ambient field=1.5 mT). The particles are slightly magnetized by the remanent field of the coils. They form small magnetic aggregates caused by the small range magnetic interaction with other particles present within small volumes of influence (magnetic capture region). Aggregate size increases with the concentration due to the reduced average interparticle distance that causes larger numbers of particles to be present within the magnetic capture regions around each particle. The pictures are taken with quasistatic conditions where the particles experience minor residual motion of the flow due to the relaxation of the tubing after injection has been stopped. Due to the quasistatic nature of the experiment, the right hand side column of Fig. 2 (high field column) shows the same particles in higher magnetic interaction configurations than in the low field column. The high field pictures were taken after magnetic aggregation reached a steady state with a magnetic field of 0.4 T. One can see greater streaking at higher field strength due to larger magnetic aggregates compared to the low field column. This is due to the fact that the magnetic capture region of each particle increased with their magnetic potential (Eq. (7)) that is a function of the higher field and higher magnetization of the particles. Similarly, to the low field column, aggregate size increases with concentration. Aggregate growth seems to occur around larger particles that attract the smallest particles toward themselves. By comparing the low and high field pictures of each concentration, it can be seen that larger particles are nuclei for cluster formation. This was illustrated using horizontal arrows connecting a few large particles of the low field column to the important aggregates that germinated around them in the high field column.

Figure 3 shows the length of aggregates major axis whose average value follows a linear trend ($R^2=0.99$) as a function of suspension concentration. The major axis length corresponds to the longest dimension of the aggregates measured on images similar to the ones depicted in Fig. 2. Larger aggregates are detected in increasing numbers as the concentration of the suspension becomes more important. Nevertheless, small aggregates still form in between the larger aggregates where the concentration appears as locally lower causing the span of the length distribution to widen with increasing concentrations. It is to note that due to contrast and resolution limitations of the microscopy setup, aggregates smaller than approximately 1 μm were difficult to detect. A bias toward larger sized aggregates is therefore expected in the data. A maximum error of approximately 10–20 μm is expected on thinnest aggregates due to limited contrast at their edges. This error is significant when it comes to distinguishing individual particles smaller than a few microns and estimating the length of the smallest aggregates. Nevertheless, it is believed to provide exploitable measurements of aggregates larger than 20–40 μm.

Figure 4 shows the area of the same aggregates measured and displayed in Fig. 3 as a function of the length of their major axis. A power regression curve superimposed on the figure yields an exponent of 1.4 ($R^2>0.9$) relating the

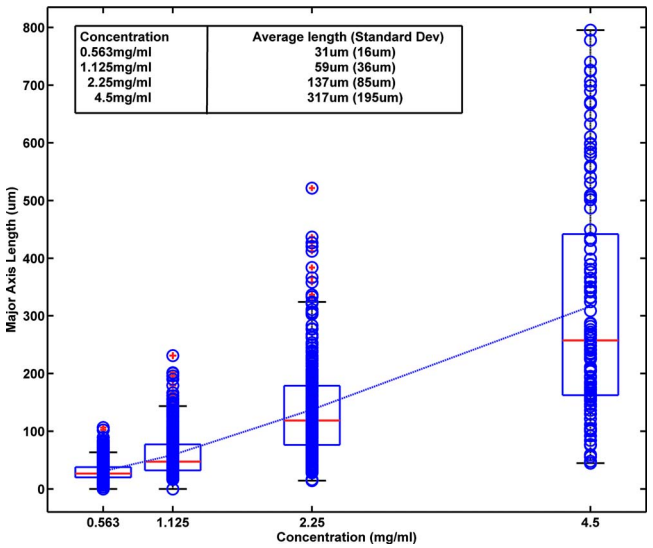

FIG. 3. (Color online) Box plots show variations in the major axis length of aggregates as a function of microparticle concentration under the influence of a 0.4 T magnetic field. The boxes have lines at the lower quartile, median, and upper quartile values. The lines (whiskers) extending from each end of the boxes show the extent of the rest of the data. Outliers (plus signs) are data with values beyond the ends of the whiskers. The data points were superimposed on the graph (circles) and a line joining the average values of each distribution was drawn.

area of the aggregates increasing with their major axis length. This exponent indicates the fact that larger aggregates have a more elongated shape. In fact, if aggregates followed an isotropic growth, one would expect a square dependence between area and length. Figure 4 also shows that aggregates with similar length but originating from different concentrations follow the same power regression. This is interpreted as an indication that the geometric proportions of aggregates depend more strongly on their length than on the concentration of the suspension.

These data demonstrate the possibility of modulating aggregate size and geometry accordingly to the experimental conditions of a given steering experiment by acting on the concentration of the suspension.

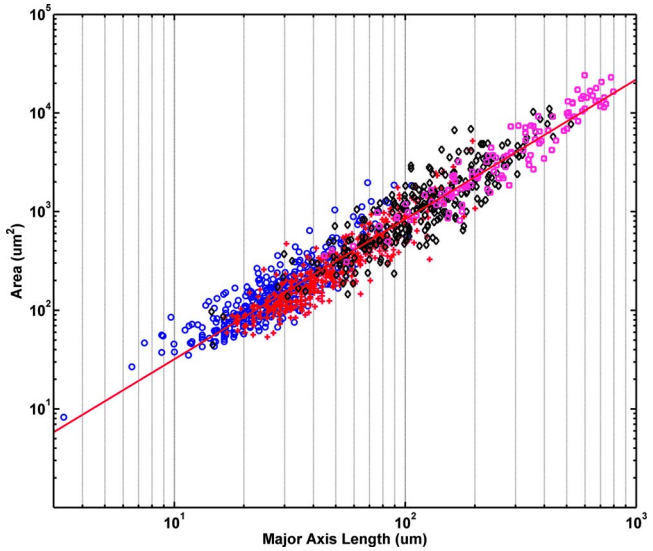

FIG. 4. (Color online) Aggregate area vs major axis length. The data originating from each concentration can be seen from left to right with a different symbol: circles (0.56 mg/ml), pluses (1.13 mg/ml), diamonds (2.25 mg/ml), and squares (4.5 mg/ml). A power regression line is drawn over the data.

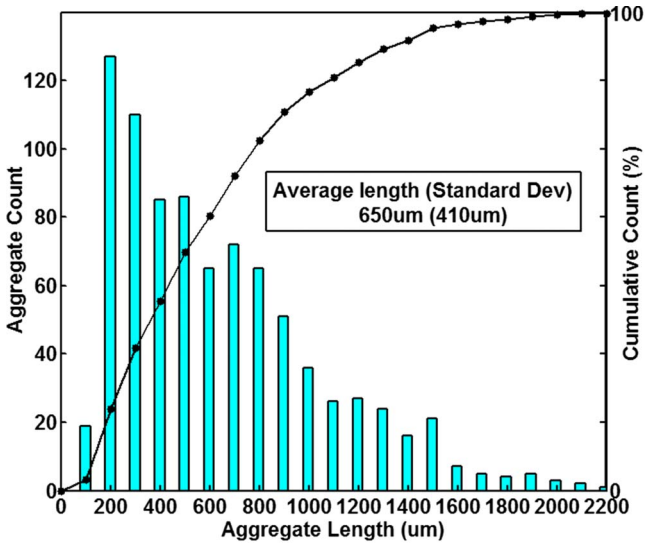

FIG. 5. (Color online) Length distribution of shear enhanced aggregation of the magnetic suspension in MRI. Suspension concentration was 1.13 mg/ml.

Low and high Mason number regimes were produced using the electromagnet setup and can be observed in video 2. Aggregate size increases if shear is applied while the magnetic field is 0.4 T. On the other hand, viscous forces overcome magnetic attraction and the aggregates collapse into single particles when shear is applied after turning the electromagnet off. In the case of the injection of the magnetic microparticles inside the bore of the MRI, shear is applied within the tubing or catheters used while a high enough magnetic field is present and low Mason numbers regimes take place. Magnetic attraction between the particles is strong enough to sustain viscous forces and orthokinetic aggregation of the existing aggregates occurs when the flow is applied. One should therefore expect a shear induced increase in aggregate size inside the bore of an MRI scanner.

High Mason numbers correspond to regimes where the shear forces are comparatively stronger than the magnetic forces. In the context of our project, high Mason regimes will occur when bringing the patient outside of the MRI scanner. The stiffness of aggregates wedged inside small arteries will drop as the magnetic interaction decreases. The aggregates are expected to break apart under the forces existing in the blood vessels and the magnetic particles would be carried farther down the vascular path they had been steered toward. If their size is sufficient, they will wedge in smaller arteries. In the opposite case, they are expected to exit the capillary network and to scatter in the vascular system.

Data of Figs. 2–4 was complemented in a low Mason number regime using the MRI setup to evaluate the effect of applying a higher and constant flow on the same suspension once static magnetization has been achieved. Figure 5 shows aggregate length measurements that were obtained through image analysis of video frames captured during the injection of the particles inside the MRI (ambient field=1.5 T). This setup was located in the highly homogeneous magnetic field of the MRI system and no magnetic gradient was applied. Therefore, the movement of the particles and aggregates was not caused by the MRI steering force induced magnetophoretic velocity. Instead, it was caused by the fluid flow, by gravity driven sedimentation to the bottom of the channel and by magnetic interactions between the particles. These effects combined with the slightly higher magnetization of the particles in the MRI magnetic field led to orthokinetic aggregation of the suspension, which caused the 1.13 mg/ml concentration to display aggregate lengths of $650+/-410$ μm as can be seen on Fig. 5 and video 3. This average length is 11 times larger than the data of Fig. 3 for the same concentration. Other effects such as width of the channels and tubing used are also expected to play significant roles such as placing a limit on the maximum size the aggregates can reach. It is to note that the average length is likely to have been overestimated since the resolution of the MRI compatible camera did not allow the measurement of the aggregates smaller than approximately 100 μm.

V. DISCUSSION

In order to tune the behavior of the suspension to the parameters of the magnetic steering experiment, one can act on each one of the following parameters: ionic content, viscosity and electromagnetic properties of the suspending fluid, the magnetic properties of the particles, their diameter, their volume fraction, and the amplitude of the magnetic field (until magnetic saturation of the particle is reached). When subjected to a flow inside the MRI, the smaller aggregates and individual particles are captured by the larger ones leading to much larger aggregates sizes. Therefore, shear and the way particles are injected in a setup are other methods the experimenter can use to affect the size and geometry of the aggregates. Of all these parameters and for a given experimental setup and magnetic suspension, the most convenient one to vary for the magnetic steering experimenter is the concentration of the particles in the suspension. Therefore, we propose the starting point of steering experiments to be the choice of a magnetic suspension followed by the tuning of aggregate size to the configuration of the magnetic steering setup by acting on the suspension's concentration.

MRI steering of magnetic microparticles is a multivariate problem. The MRI compatible size measurement method and the list of the parameters that can be used to affect aggregates size and geometry proposed here are the tools required to assess whether aggregate dimensions are appropriate to the pursued arterial size range. As described, magnetic aggregation significantly affects the magnetophoretic velocity achieved by magnetic particles. Future works to model the magnetophoretic velocity of aggregates will need to be carried out to study several parameters in more detail: aggregate volume and density (3D fractal dimension) in order to better estimate the magnetic force, geometry and 3D aggregate hydrodynamic diameter tensor for viscous drag calculation, viscous wall retardation effect, and friction force between the particles/aggregates and channels walls as a function of the angle between the flow and the direction of magnetization since these forces work against the magnetic force. Finally, adverse effects such as viscous resuspension[29] and diffusion might play significant roles in some cases.

Since magnetic aggregation of the particles in MRI steering appears inevitable, the experimenter must try to make the most of it and get it to affect the steering efficiency in the most positive way possible. The application of this MRI steering technology being chemoembolization, the maximum size of the clusters must be set by the lumen of the smallest vessels the experimenter wants to target. Standard particles for transcatheter arterial embolization and transcatheter arterial chemoembolization are as large as several hundreds of micrometers.[30,31] Magnetic aggregation appears to be a valid solution to the design constraints originating from the wide range of physiological parameters existing in the vascular system. As a matter of fact, in the context of MRI targeted chemoembolization, magnetic particles need to flow from millimeter sized arteries with flow velocities as high as several tens of cm/s to vessels as small as $5-100$ μm with flow velocities below 1 cm/s. Individual particles small enough to flow through the microcirculation will not be adapted to larger arteries due to their low magnetophoretic velocity. On the other hand, a particle large enough to sustain the flow of large arteries will embolize prematurely and will not be able to reach the vicinity of a tumor. Magnetic suspensions with controlled aggregation properties could be designed in order to form aggregates adapted to large arteries upon injection. While reaching smaller vessels, the design of the particles would cause the aggregates to dissolve in order to comply with the geometry of the vascular system. When the individual particles reach vessels with small enough sizes, they will wedge and perform the embolization therapy. The compliance of magnetic aggregates with vessel geometry will have to be studied in more details in order to define the design parameters of the particles (Mason number, magnetic moment, surfactants, and colloidal properties).

VI. CONCLUSION

Throughout this study, we worked at identifying the parameters and studying the phenomenon of magnetic aggregation in the context of MRI guidance of magnetic particles. Experiments were conducted on the aggregation of magnetic particles in a magnetic field. The data obtained demonstrate that aggregating particles form clusters with a longer axis oriented along the direction of the magnetic field. With the electromagnet setup, their average length appeared to be a linear function of the suspension concentration. The application of shear can either lead to aggregate collapse or growth depending on the balance between shear forces and magnetic forces. Aggregation can facilitate magnetic steering by increasing the influence of the magnetic propulsion force over the viscous friction forces. Future work should include precise estimations of the magnetophoretic velocity of magnetic aggregates, the fraction of aggregated versus nonaggregated particles, and the compliance of the aggregates.

ACKNOWLEDGMENTS

This project is supported in part by a Canada Research Chair (CRC) in Micro/Nanosystem Development, Fabrication and Validation, the Canada Foundation for Innovation (CFI), the National Sciences and Engineering Research Council of Canada (NSERC), Fonds Québécois de la Recherche sur la Nature et les Technologies (FQRNT), and the Government of Québec. The authors wish to acknowledge the assistance of Pierre Pouponneau in the MRI experiments, static light scattering, and VSM measurements, Charles C. Tremblay for his assistance in the design of the fluidic channels, Pr. Basil D. Favis and Pierre Le Corroller for their assistance with aggregate size measurement, Pr. David Ménard for his kind counsel and for allowing access to his research facilities, VSM and electromagnets and Hôpital Notre Dame for allowing access to the MRI scanner.

[1] S. Odenbach, *Magnetoviscous Effects in Ferrofluids* (Springer, New York, 2002).
[2] S. Genç and P. P. Phule, Smart Mater. Struct. **11**, 140 (2002).
[3] K. Parekh, R. Patelb, R. V. Upadhyayb, and R. V.Mehta, J. Magn. Magn. Mater. **289**, 311 (2005).
[4] M. Piao, A. M. Lane, and D. T. Johnson, J. Magn. Magn. Mater. **267**, 366 (2003).
[5] J. Popplewell and L. Sakhnini, J. Magn. Magn. Mater. **149**, 72-78 (1995).
[6] H. Shahnazian and S. Odenbach, J. Phys.: Condens. Matter **20**, 204137 (2008).
[7] R. E. Rosensweig, *Ferrohydrodynamics* (Dover, Mineola, New York, 1997).
[8] C. Alexiou, W. Arnold, P. Hulin, R. J.Klein, H. Renz, F. G. Parak, C. Bergemann, and A. S. Lübbe, J. Magn. Magn. Mater. **225**, 187 (2001).
[9] M. Shinkai, J. Biosci. Bioeng. **94**, 606 (2002).
[10] H. Nobuto, T. Sugita, T. Kubo, S. Shimose, Y. Yasunaga, T. Murakami, and M. Ochi, Int. J. Cancer **109**, 627 (2004).
[11] A. J. Lemke, M.-I. Senfft von Pilsach, A. Lübbe, C. Bergemann, H. Riess, and R. Felix, Eur. Radiol. **14**, 1949 (2004).
[12] E. Virooncharapan, M. Ueno, H. Sato, I. Adachi, H. Nagae, K. Tazawa, and I. Horikoshi, Pharm. Res. **12**, 1176 (1995).
[13] Ch. Alexiou, A. Schmidt, R. Klein, P. Hulin, Ch. Bergemann, and W. Arnold, J. Magn. Magn. Mater. **252**, 363 (2002).
[14] J.-H. Seppenwoolde, J. F. W. Nijsen, L. W. Bartels, S. W. Zielhuis, A. D. van het Schip, and C. J. G. Bakker, Magn. Reson. Med. **53**, 76 (2005).
[15] S. Martel, J.-B. Mathieu, O. Felfoul, A. Chanu, É. Aboussouan, S. Tamaz, P. Pouponneau, G. Beaudoin, G. Soulez, L'H. Yahia, and M. Mankiewicz, Appl. Phys. Lett. **90**, 114105 (2007).
[16] O. Felfoul, J.-B. Mathieu, G. Beaudoin, and S. Martel, IEEE Trans. Med. Imaging **27**, 28 (2008).
[17] J. B. Mathieu and S. Martel, Biomed. Microdevices **9**, 801 (2007).
[18] A. Chanu, O. Felfoul, G. Beaudoin, and S. Martel, Magn. Reson. Med. **59**, 1287 (2008).
[19] S. Tamaz, A. Chanu, J.-B. Mathieu, R. Gourdeau, and S. Martel, IEEE Trans. Biomed. Eng. **55**, 1854 (2008).
[20] N. J. Darton, A. J. Sederman, A. Ionescu, C. Ducati, R. C. Darton, L. F. Gladden, and N. H. Slater, Nanotechnology **19**, 395102 (2008).
[21] C.-J. Chin, S.-C. Lu, S. Yiacoumi, and C. Tsouris, Sep. Sci. Technol. **39**, 2839 (2004).
[22] C.-J. Chin, S. Yiacoumi, and C. Tsouris, Langmuir **17**, 6065 (2001).
[23] C. Tsouris and T. C. Scott, J. Colloid Interface Sci. **171**, 319 (1995).
[24] M. Aoshima and A. Satoh, J. Colloid Interface Sci. **288**, 475 (2005).
[25] A. O. Ivanov and S. S. Kantorovich, Kolloidn. Zh. **65**, 166 (2003).
[26] E. Brunet, G. Degre, F. Okkels, and P. Tabeling, J. Colloid Interface Sci. **282**, 58 (2005).
[27] A. Zubarev and L. Iskakova, J. Phys.: Condens. Matter **20**, 204138 (2008).
[28] A. Yu Zubarev and L. Yu. Iskakova, Physica A **382**, 378 (2007).
[29] D. Leighton and A. Acrivos, Chem. Eng. Sci. **41**, 1377 (1986).
[30] S. Virmani, D. Wang, K. R. Harris, R. K. Ryu, K. T. Sato, R. J. Lewandowski, A. A. Nemcek, B. Szolc-Kowalska, G. Woloschak, R. Salem, A. C. Larson, and R. A. Omary, J. Vasc. Interv. Radiol. **18**, 1280 (2007).
[31] R. J. Lewandowski, D. Wang, J. Gehl, B. Atassi, R. Ryu, K. Sato, A. Nemcek, Jr., F. Miller, M. Mulcahy, L. Kulik, J. Vasc. Interv. Radiol. **18**, 1249 (2007).